Received: 5 May 2021 | Revised: 10 August 2021 | Accepted: 7 September 2021

DOI: 10.1096/fj.202100753R

THE FASEB JOURNAL

RESEARCH ARTICLE

PTENα is responsible for protection of brain against oxidative stress during aging

Pan Wang[1,2] | **Ruiqi Li**[3] | **Yuyao Yuan**[1] | **Minglu Zhu**[1] | **Yang Liu**[1] | **Yan Jin**[1] | **Yuxin Yin**[1,3]

[1]Department of Pathology, School of Basic Medical Sciences, Institute of Systems Biomedicine, Peking University Health Science Center, Beijing, China

[2]Tsinghua University-Peking University Joint Center for Life Sciences, Tsinghua University, Beijing, China

[3]Peking-Tsinghua Center for Life Sciences, Peking University, Beijing, China

Correspondence
Yuxin Yin, Department of Pathology, School of Basic Medical Sciences, Institute of Systems Biomedicine, Peking University Health Science Center, Beijing 100191, China.
Email: yinyuxin@hsc.pku.edu.cn

Funding information
National Natural Science Foundation of China, Grant/Award Number: 81430056, 31420103905, 81621063 and 31800849; National Key Research and Development Program of China, Grant/Award Number: 2016YFA0500302; Beijing Natural Science Foundation Key Grant, Grant/Award Number: 7161007; China Postdoctoral Science Foundation, Grant/Award Number: 2017M620006

Abstract

Neural cells are continuously subjected to oxidative stress arising from electrochemical activity, and cellular protection systems can turn on the oxidative stress response to detect and alleviate adverse conditions. However, the function and mechanism of the protective systems are complicated and remain largely elusive. We report that PTENα, an isoform of the PTEN family, mediates defense signaling in response to oxidative stress during brain aging. We show that genetic ablation of *Ptenα* in mice increases oxidative stress and results in neuronal cell death, culminating in accelerated decline of cognition and motor coordination as age increases. PTENα maintains COX activity and promotes energy metabolism through abrogating NEDD4L-mediated degradation of COX4 in response to oxidative stress. In the presence of Parkinson's disease-associated mutation, PTENα loses the capability to protect COX4 and ameliorate defects caused by Ptenα deletion. Our study reveals an important role of PTENα in response to oxidative stress. We propose that dysregulation of PTENα signaling may accelerate the rate of brain aging and promote the development of neurodegenerative disorders.

KEYWORDS
aging, COX4, oxidative stress, PTENα

Abbreviations: AAV, adeno-associated virus; AD, Alzheimer's disease; CaMKIIα, Ca^{2+}/calmodulin-dependent protein kinase II α; COX, cytochrome c oxidase; CRISPR/Cas9, clustered regularly interspaced short palindromic repeats/caspase-9; DHE, dihydroethidium; GNB2, G protein subunit beta 2; NEDD4, NEDD4 E3 ubiquitin protein ligase; NEDD4L, NEDD4 like E3 ubiquitin protein ligase; NOR, novel object recognition; NRF2, nuclear factor erythroid 2-related factor; OB, olfactory bulb; PD, Parkinson's disease; PTENα, phosphatase, and tensin homolog deleted on chromosome ten α; ROS, reactive oxygen species; STUB1, STIP1 homology and U-Box containing protein 1; TUNEL, terminal-deoxynucleoitidyl transferase mediated nick end labeling; UBE4A, ubiquitination factor E4A; UBE4B, ubiquitination factor E4B.

Pan Wang and Ruiqi Li contributed equally to this work.

1 | INTRODUCTION

Several potential risk factors including aging, oxidative stress, genomic defects, inflammation, epigenetic modification, and environmental aspects have been reported to be involved in the pathogenic processes of neurodegenerative diseases.[1,2] Among them, the greatest risk factor is aging. The physiological integrity of the brain declines progressively during aging, which is characterized by decrements in sensory perception, attention, decision-making speed, learning-memory, and motor coordination.[3–5] As individuals age, they become increasingly prone to developing a neurodegenerative disorder, and the most common cases are Alzheimer's disease (AD) and Parkinson's disease (PD).[6,7] Studies have revealed multiple hallmarks of brain aging at the molecular, cellular, and systemic level, these hallmarks include mitochondrial dysfunction, dysregulated energy metabolism, and impaired adaptive stress response signaling etc.[8–11]

To protect neuronal cells from being damaged by oxidative stress, the nervous system possesses numerous conserved stress response pathways to detect and alleviate a wide range of adverse conditions, alert surrounding cells to stress situations and strengthen defenses against impending stressors. For example, if reactive oxygen species (ROS) abnormally accumulate in cells, these ROS function as signaling molecules to activate the oxidative stress response to stabilize the transcription factor nuclear factor erythroid 2-related factor (NRF2).[12] NRF2 induces the expression of proteins that scavenge oxidizing molecules and eliminate or repair oxidized proteins.[13] Stress response pathways are impaired during aging, and ultimately increase the vulnerability to develop neurodegenerative diseases.[14]

Imbalance between the generation and clearance of ROS results in oxidative stress and provokes cell death.[15,16] The major site of production of ROS is the mitochondrial respiratory chain, which is composed of four complexes: complex I, complex II, complex III, and complex IV (cytochrome *c* oxidase, COX).[17,18] Inhibition of complex I, complex III, or complex IV enhances the formation of hydrogen peroxide in mitochondria,[18,19] implying the necessity to maintain the activity of these complexes. Cytochrome c oxidase (COX) increases the transmembrane difference of proton electrochemical potential to promote ATP production.[20] Most COX-related disorders are linked to mutations in nuclear-encoded proteins, which contribute to COX structure and functionality.[21–24] The increased reliance of neurons on oxidative phosphorylation for energy facilitates the use of COX histochemistry in mapping regional brain metabolism in animals since it establishes a direct and positive correlation between the enzyme activity and neuronal activity.[24–27] This can be seen in the correlation between COX enzyme amount and activity, which indicates the regulation of COX is at the gene expression level. COX4 (Cytochrome c oxidase subunit 4i1, COX4i1) is the largest subunit among ten nuclear-encoded subunits and has been reported to be a required component of COX biogenesis.[28,29] However, function and regulation of COX4 in the brain remain largely unknown.

We have specialized in the identification of isoforms of the PTEN family and the investigation of their specific roles in biologic processes. PTENα is the longest isoform of PTEN that translates from a nonclassical start codon CUG and, compared to PTEN, contains an evolutionarily conserved extended 173-aa N-terminus.[30,31] Several studies have revealed the extended N-terminus confers multiple specific functions to PTENα: maintaining mitochondrial energy metabolism through the Parkin-Pink1 pathway[31]; regulating fear-conditioned memory through CaMKIIα signaling[32]; and participating in olfaction process by modulating endocytosis.[33] Diminished olfaction is a common feature of aging and our preliminary data showed PTENα gradually declines with increasing age in mouse olfactory bulb (OB),[33] raising the possibility that PTENα decline might associate with aging process.

Another important feature of brain aging is inter-individual variability. There are undoubtedly genetic factors that influence the rate of brain aging. In this study, we show that PTENα-deficient mice recapitulate multiple pathologic features of aging, including accelerated cognitive and motor coordination decline, and aberrant cell death in the midbrain. These observations lead us to determine whether PTENα is one of the genetic factors that account for brain aging.

2 | MATERIALS AND METHODS

2.1 | Animals

Ptenα specific knock-out mouse strain was generated and maintained as previously reported.[32] All the animal study protocols followed the Peking University Guidelines for "Using Animals in Intramural Research" and were approved by the ethics committee of Peking University Health Science Center.

2.2 | Cell lines, plasmids generation and transfection

Cell lines HEK293T, SH-SY5Y, and Hela were obtained from the American Type Culture Collection and cultured in DMEM supplemented with 10% (vol/vol) FBS at 37°C in

a humidified 5% CO_2 atmosphere (Thermo). $COX4^{+/-}$ SH-SY5Y cell line was generated by CRISPR/Cas9 technology. The single guide RNA (sgRNA) sequence targeting human *COX4* was designed using the CRISPR design tool at http://crispr.mit.edu/. The guide sequence was 5′-GACCAGGGTATTTAGCCTAGT-3′, and this sequence was cloned into pX330 vector. SH-SY5Y cells were seeded onto 6-well plates (Corning) at a density of 1×10^5 cells/well. The sgRNA and cas9 were co-transfected into SH-SY5Y cells followed by screening with G418 (INALCO, 1758-1811). Cell clones were further picked and amplified for sequencing of genomic DNA using the following primers: forward-5′-GGATCATTTGCGTTGGGGAGAAGCA-3′.

COX4 plasmid was constructed by sub-cloning human COX4 cDNA (including full-length and mutants) into pSA-HA-S-tag vector. PTENα plasmids were described in previous studies.[31,32] NEDD4L plasmids were gift from prof. Tao's lab in Tsinghua university. Plasmids used in experiments were extracted using M5 Plasmid Miniprep plus Kit (Mei5bio, MF031-plus-01). Transfection of plasmids was performed with Polyethyleneimine (PEI), TransIntroTM EL Transfection Reagent (Transgene, FT201), or Lipofectamine 3000 (Invitrogen, L3000015) according to the manufacturer's instruction.

2.3 | Antibodies and drugs

The following antibodies and drugs were used in this study: anti-PTEN (CST, #9559S), anti-GAPDH (Sungene Biotech, KM9002T), anti-FLAG (Sigma-Aldrich, F3165), anti-HA (Sigma-Aldrich, H3663), anti-Myc (Santa cruz, sc-40), anti-COX4 (Ruiying, RLT1074), anti-NEDD4L (proteintech,13690-1-AP), MG132 (Dalian Meilun, MB5137), CHX (Pharma biology, C21865), Protease inhibitor cocktails (LABLEAD, C0101), and Phosphatase inhibitor cocktail (Bimake, B15002).

2.4 | Myc pull-down and S-tag pull-down assays

HEK293T cells transfected with Myc-tagged or S-tagged plasmids for 24 h. Cells were harvested and lysed in 0.5% NP-40 lysis buffer containing 150 mM NaCl, 2 mM EDTA, 50 mM Tris-HCl, 0.5% NP-40 supplemented with protease and phosphatase cocktails. Supernatants obtained after centrifugation at 12 000 rpm for 15 min at 4°C. For evaluation of protein interaction: supernatants were incubated with anti-Myc-beads (MBL, M047-11) or S-protein Agarose (EMD Millipore Corp., Billerica, MA USA, 69704-4) overnight (>8 h) at 4°C. For evaluation of protein ubiquitination: supernatants were added with SDS to a final concentration at 1% and boiled at 95°C for 15 min. Supernatants then were incubated with S-protein agarose overnight (>8 h) at 4°C. Precipitants were washed 3 times with 0.1% NP-40 buffer (150 mM NaCl, 2 mM EDTA, 50 mM Tris-HCl, and 0.1% NP-40 supplemented with protease and phosphatase cocktails) and subjected to immunoblots.

2.5 | Mitochondria activity assay and ATP production assay

The mitochondria from cells or tissues were extracted with the ProteoExtract® cytosol/mitochondria fractionation kit (Merck, QIA88) according to the manufacturer's protocol. The mitochondria activity assay (Cytochrome C oxidase activity assay) kit (BioChain, KC310100) and ATP bioluminescent assay kit (BioAssay Systems, EATP006) were used for determination of COX activity and ATP production in extracted mitochondria. The detection process was performed according to the manufacturer's protocol.

2.6 | Lentivirus packaging and infection

The pLKO.1.5-TRC lentiviral shRNA system from Tsinghua University shRNA library was used for NEDD4L knockdown. The oligo sequences of shRNA targeting human *NEDD4L* are as follows: #1:5′-CCGGCGCCTTGACTTACCTCCATATCTCGAGATATGGAGGTAAGTCAAGGCGTTTTT-3′, #2:5′- CCGGGCGGATGAGAATAGAGAACTTCTCGAGAAGTTCTCTATTCTCATCCGCTTTTT-3′, #3:5′- CCGGGCGAGTACCTATGAATGGATTCTCGAGAATCCATTCATAGGTACTCGCTTTTT-3′. pLKO.1.5-shNEDD4L, pAX.2, and pMD.2G were co-transfected into HEK293T cells at a ratio of 6:3:1 for 48 h, then collecting cell culture media. The virus supernatant with polybrene (8 μg/ml) was added into the culture medium (1:1) for 24 h. Puromycin (4 μg/ml) was used for sorting and selecting positive cells.

2.7 | Behavioral tests

All behavioral tests were performed with male mice under dim conditions, and mice were moved to a holding room in the behavioral testing area at least 1 h prior to the beginning of the tests. Apparatuses were cleaned with 75% ethanol. Manual scoring was performed by a trained observer blind to genotype; automatic scoring was performed using the Ethovision XT v.13 software (Noldus).[34] Details of these paradigms are listed below.

2.8 | Rotarod test

Mice were placed on the rod and the speed of the rotation gradually accelerated from 4 to 40 rpm/min over a 5 min period. Mice received three trials, spaced at least 10 min apart. Their latency to fall to the bottom of the chamber was measured (averaged across tests).

2.9 | Novel object recognition

Mice were habituated to the experimental arena without stimuli for 15 min daily for 3 days before the commencement of behavioral tests. The procedure consists of a sample phase, followed by a preference test after a delay of 24 h. For the sample phase, mice were placed in the apparatus with two identical objects and allowed to explore for 10 min. During the test phase, mice were presented with an old object from the sample phase and one novel object for 5 min. All objects were thoroughly cleaned between trials to ensure olfactory signals would not confound the results. Time spent exploring each object was subsequently automatic scored, and an animal's performance in novel object recognition memory was assessed by a discrimination ratio.

2.10 | Stereotactic injection of adeno-associated virus (AAVs)

Mice were anesthetized with 1% isofluorane and positioned in a stereotactic frame. Each mouse was bilaterally injected with virus stock solution (titer AAV-EGFP: 4.1×10^{13}, 100 nl; AAV-PTENα: 1.69×10^{13}, 240 nl; AAV-PTENα^{H169N}: 2.39×10^{13}, 170 nl; OBiO Technology) at a rate of 0.04 μl/min using a 10 μl micro-syringe (Hamilton, NRS1701 RN 10 μl) with a 33 gauge needle (Hamilton, NRS NDL RN 6/PK), which was controlled by a microsyringe pump (UMP3; WPI) and its controller (Micro4; WPI). The coordinates for the midbrain were: AP −2.4 mm; ML ±1.1 mm; DV 3.6 mm. After injection, the needle was maintained in place for an additional 5 min and then slowly withdrawn. Mice underwent post-surgery recovery for 4 weeks before behavioral tests.

2.11 | TUNEL staining

Mice brains were prepared as paraffin-embedded slices (5 μm, coronal plane). Slices were dewaxed with xylene at room temperature (RT) for 5 min/time, 3 times, and then treated with 100%, 80%, 70% EtOH for 5 min respectively. Samples were rinsed with 1× PBS before permeabilization within 0.1% Triton X-100 in 0.1% sodium citrate tribasic dihydrate at RT for 10 min. Positive control was incubated in DNase solution (50 mM Tris-HCl pH 7.5, 10 mM $MgCl_2$, 1 mg/ml BSA in 1× PBS, DN25 powder was dissolved at a concentration of 1 mg/5 ml) at 37°C for 10 min, while normal samples were moistened by 1× PBS. Then, each sample was incubated with 30 μl TUNEL reaction mixture (in situ cell death detection kit POD, Roche) for 60 min at 37°C, while negative control was only added with label solution and covered with coverslip. After, rinsed slices with 1× PBS for 5 times, 5 min/time. Slices were mounted and analyzed by fluorescence microscopy (Nikon TCS A1 microscope).

2.12 | DHE staining

ROS levels in tissues were evaluated by staining cryostat sections of brain tissue (30 μm) with dihydroethidium (DHE, D11347, Invitrogen). Sections were reacted with 5 μM DHE at RT for 30 min under protection from light, and then washed with ice cold 1× PBS, and mounted with anti-quenching reagent. Fluorescence was measured with excitation at 488 nm and emission in the range of 590–610 nm, using a fluorescent microscope (Olympus IX51).

Evaluation of ROS generation in cells: cells were seeded in 6-well plate 5×10^5/well 24 h before detection. Cells were washed gently with ice cold 1× PBS for 3 times, and then incubated in 5 μM DHE at 37°C for 15 min in cell incubator. After that, cells were washed with 1× PBS for 3 times to remove excessive DHE and observed under a fluorescent microscope (Olympus, IX51). Cells that had bright fluorescent red was defined as ROS-positive. Images taken under brightfield were used to count as total cell number. The mean optical density of DHE signal was expressed as red florescent density (measured by image J software) versus total cell number. At least 5 different visual field images per group were used for statistics analysis.

2.13 | Statistical analysis

Densitometric quantification of immunoblotting levels was performed using Quantity One software. Statistical analysis was performed with Prism GraphPad software v6.01. The statistical significance of differences between groups was calculated with the two-tailed unpaired or paired *t*-test, one-way analysis of variance (ANOVA) followed by Turkey's post hoc comparison, or two-way ANOVA followed by Bonferroni or Turkey correction for multiple comparisons. Error bars represent standard error of the mean (SEM). *p*-Values of .05 or less were considered statistically significant. $^{*}p < .05$, $^{**}p < .01$, $^{***}p < .005$, and $^{****}p < .0001$.

3 | RESULTS

3.1 | PTENα increases with moderate stimulation of oxidative stress and declines with increasing age

To investigate the response of PTENα to oxidative stress, H_2O_2 was used to induce aberrant oxidative stress in cells. PTENα$^{+/+}$ and PTENα$^{-/-}$ Hela cells, which were generated in our previous study,[31] were incubated with different doses of H_2O_2, and the levels of endogenous PTENα were detected with a commercial PTEN antibody. We noticed that PTENα levels gradually increased within a range of low doses of H_2O_2 (Figure 1A, lane 1 vs. lane 3 vs. lane 5, and Figure 1B), and subsequently declined with an overdose of H_2O_2 in PTENα$^{+/+}$ Hela cells (Figure 1A, lane 7 vs. lane 5), whereas PTEN levels remained unchanged (Figure 1A,B). Moreover, a low dose of H_2O_2 significantly increased the expression levels of PTENα in a time-dependent manner without affecting PTEN levels (Figure 1C, lane 1 vs. lane 3 vs. lane 5, and Figure 1D). These results suggest that PTENα is an oxidative stress response factor.

Ptenα is predominantly expressed in the brain, especially in the OB, midbrain, cortex, and hippocampus.[32] Our preliminary data has shown Ptenα levels in the OB gradually declined with increasing age after adulthood.[33] Ptenα expression patterns in mouse midbrain, cortex, and hippocampus were further evaluated. As age increased, Ptenα levels displayed an obvious reduction (Figure 1E,F). It is worth noting that oxidative stress becomes severe with increasing age, this means oxidative stress takes place with an opposite spatial and temporal pattern to Ptenα, raising the possibility that there might exist a relationship between Ptenα and oxidative stress during aging.

The impact of PTENα ablation on oxidative stress state, which could be reflected by cellular ROS levels, was further determined. We performed dihydroethidium (DHE) staining to monitor cellular ROS in PTENα$^{+/+}$ and PTENα$^{-/-}$ Hela cells. DHE describes the superoxide content within cells in the forms of red fluorescence, and enhanced red fluorescence intensity occurred in PTENα$^{-/-}$ Hela cells (Figure 1G,H), demonstrating that the loss of PTENα results in an elevation of oxidative stress in cells. These data together imply that PTENα may be involved in the antioxidant process.

3.2 | Ptenα ablation aggravates oxidative stress and age-related behavioral dysfunction in mice

As previously described, we have generated a Ptenα-specific knockout mouse model by substituting the two initiation codons of *Ptenα* (CTG347 and CTG362) with GGA. Mice with completed deletion of *Ptenα* are designated as *Ptenα*$^{mu/mu}$, and their wild-type littermates are *Ptenα*$^{+/+}$ mice.[32] Mice used for our subsequent experiments were genotyped by PCR, in which the mutant allele was longer than the wild-type allele (Figure S1A, lane 2 vs. lane 3). We further verified ablation of Ptenα in the brain through immunoblotting. Ptenα was completely deleted in *Ptenα*$^{mu/mu}$ mice, whereas PTEN level was unaffected (Figure S1B, lanes 2, 4, 6, 8 vs. lanes 1, 3, 5, 7). To determine whether oxidative stress status was influenced by Ptenα deletion in vivo, DHE staining with brain tissue cryosections was performed to evaluate ROS levels in *Ptenα*$^{+/+}$ and age-matched *Ptenα*$^{mu/mu}$ mice. By screening the whole brain section, the intensity of red fluorescence was prominently elevated in the midbrain of 6-month-old *Ptenα*$^{mu/mu}$ mice (Figure 2A–C), indicating that deletion of Ptenα increases oxidative stress in mouse midbrain. We therefore focused on midbrain for subsequent investigation.

ROS generally cause DNA damage and even neuronal death, which marks the irreversible deterioration of the nervous system,[35] raising the possibility that the loss of Ptenα would induce further cellular damage in vivo. To address this question, we performed terminal-deoxynucleotidyl transferase mediated nick end labeling (TUNEL) enzymatic staining with brain cryosections from *Ptenα*$^{+/+}$ and *Ptenα*$^{mu/mu}$ mice. Positive green fluorescence signals were clearly detected in the midbrain of 10-month-old *Ptenα*$^{mu/mu}$ mice (Figure 2D, middle panel). However, these signals were nearly absent in the midbrain of control (Figure 2D, left panel) as well as the hippocampus of *Ptenα*$^{mu/mu}$ mice (Figure 2D, right panel). Quantification showed an approximately three-fold increase in the percentage of cell death in the midbrain of *Ptenα*$^{mu/mu}$ mice (Figure 2E), suggesting Ptenα depletion exacerbates cellular damage in mouse midbrain.

To determine whether Ptenα ablation influences the function of midbrain, we conducted rotarod test to assess general motor coordination and balance in mice. Mice at different ages were tested on the rotarod and a shorter latency to fall indicated impaired motor coordination and balance. Planned comparisons found no differences within *Ptenα*$^{mu/mu}$ and *Ptenα*$^{+/+}$ young mice (Figure 2F, 2-month-old). When mice got older, *Ptenα*$^{mu/mu}$ mice dropped from the rotarod faster than *Ptenα*$^{+/+}$ cohorts did (Figure 2F, 6-month-old). Furthermore, this difference became more obvious between 10-month-old *Ptenα*$^{mu/mu}$ and *Ptenα*$^{+/+}$ mice (Figure 2F). These data strongly suggest Ptenα-deficient mice are prone to displaying motor dysfunction as age increased.

We also carried out novel object recognition (NOR) to evaluate the cognitive ability, which was indicted by discrimination index. During this test, a retention trial

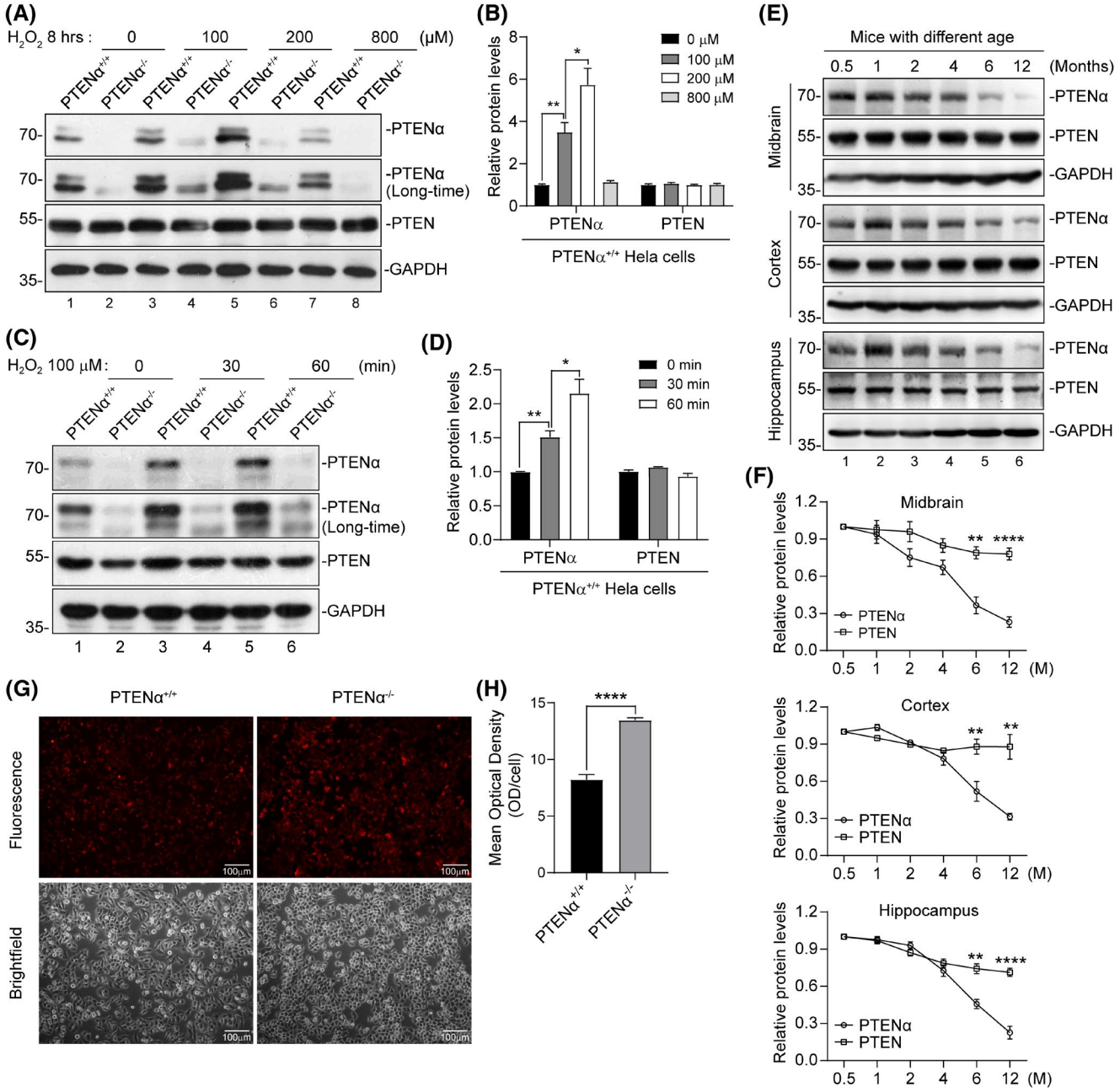

FIGURE 1 PTENα increases following H_2O_2 treatment and decreases in mouse brain as age increased. (A) Immunoblot analysis for PTENα, PTEN, and GAPDH performed with lysates from PTENα$^{+/+}$ and PTENα$^{-/-}$ Hela cells treated as indicated. Blots are representative of 3 independent experiments. (B) Relative protein levels of PTENα and PTEN in PTENα$^{+/+}$ cells normalized to GAPDH. Cells were treated as indicated in (A). Data in (B) are means ± SEM from 3 independent experiments. *p* Values are determined by one-way ANOVA followed by Tukey's post hoc test. (C) Immunoblot analysis for PTENα, PTEN, and GAPDH protein levels in PTENα$^{+/+}$ and PTENα$^{-/-}$ Hela cells treated as indicated. Blots are representative of 3 independent experiments. (D) Relative protein levels of PTENα and PTEN in PTENα$^{+/+}$ cells normalized to GAPDH. Cells were treated as indicated in (C). Data in (D) are means ± SEM from 3 independent experiments. *p* Values are determined by one-way ANOVA followed by Tukey's post hoc test. (E) Immunoblot analysis of PTENα, PTEN, and GAPDH in the midbrain, cortex, and hippocampus of mice at age as indicated. Blots are representative of 3 independent experiments. (F) Relative protein levels of PTENα and PTEN in mice normalized to GAPDH. Data are means ± SEM from 3 independent experiments. Mice $n = 3$ per timepoint. M, months. *p* Values are determined by one-way ANOVA followed by Tukey's post hoc test. (G) Representative images of DHE staining to assess ROS levels (Red fluorescence) in PTENα$^{+/+}$ and PTENα$^{-/-}$ Hela cells. Scale bar, 100 μm. DHE, dihydroethidium. ROS, Reactive oxygen species. (H) Quantification of ROS levels in PTENα$^{+/+}$ and PTENα$^{-/-}$ Hela cells was achieved by measuring mean optical density (OD/cell) of DHE signal using image J software. Data in (H) are means ± SEM, $n = 3$ independent experiments with 1×10^4 cells in total from PTENα$^{+/+}$ and PTENα$^{-/-}$ cells respectively. *p* Values are determined by unpaired *t* tests. *$p < .05$, **$p < .01$, ****$p < .0001$

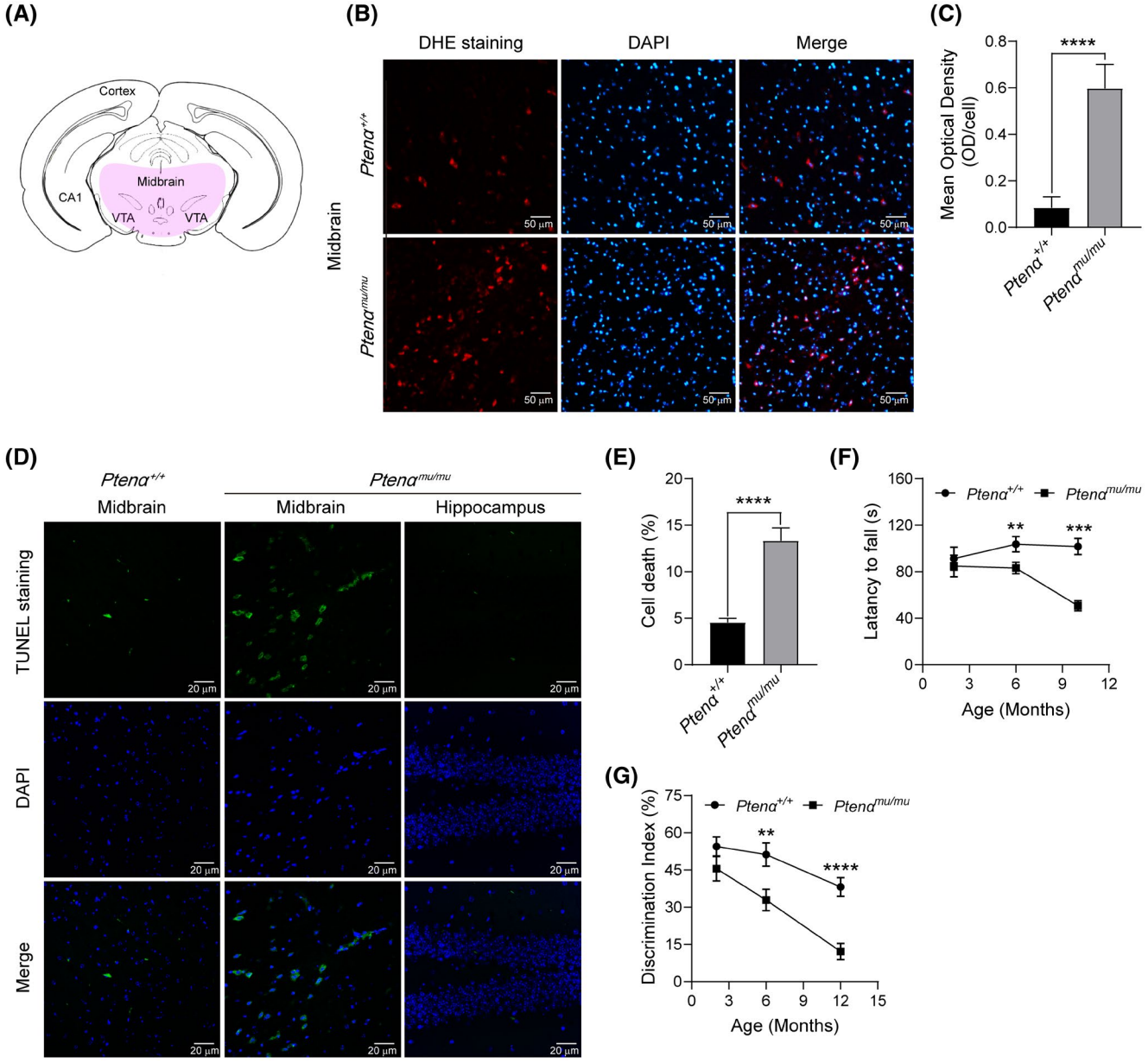

FIGURE 2 Pathological and behavioral changes in *Ptenα*$^{mu/mu}$ mice. (A) Schematic indication of mouse midbrain region, which was marked with purple. CA1, field CA1 of hippocampus. VTA, ventral tegmental area. (B) Representative images from DHE stained midbrain sections of 6-month-old *Ptenα*$^{+/+}$ and *Ptenα*$^{mu/mu}$ mice. Scale bar, 50 μm. DAPI, 4′,6-diamidino-2-phenylindole. (C) Quantification of ROS formation in the midbrain of *Ptenα*$^{+/+}$ and *Ptenα*$^{mu/mu}$ mice were achieved by measuring mean optical density values of DHE signal from >200 cells using image J software. Data are shown as mean ± SEM, mice $n = 3$ per genotype. p Values are determined by unpaired t tests. (D) Representative images of TUNEL staining to assess cell death (green fluorescence) in the midbrain of 10-month-old *Ptenα*$^{+/+}$ and *Ptenα*$^{mu/mu}$ mice. Scale bar, 20 μm. TUNEL, terminal-deoxynucleoitidyl transferase mediated nick end labeling. (E) Quantification of TUNEL signal positive cells in the midbrain of *Ptenα*$^{+/+}$ and *Ptenα*$^{mu/mu}$ mice. Percentage of cell death was analyzed. Data are shown as mean ± SEM, mice $n = 3$ per genotype. p Values are determined by unpaired t tests. (F) Latency to fall of *Ptenα*$^{+/+}$ and *Ptenα*$^{mu/mu}$ mice in rotarod test. Data are shown as mean ± SEM, 2-month-old group: $n = 9$ *Ptenα*$^{+/+}$ mice, $n = 11$ *Ptenα*$^{mu/mu}$ mice; 6-month-old group: $n = 7$ *Ptenα*$^{+/+}$ mice, $n = 7$ *Ptenα*$^{mu/mu}$ mice; 10-month-old group: $n = 9$ *Ptenα*$^{+/+}$ mice, $n = 9$ *Ptenα*$^{mu/mu}$ mice. p Values are determined by two-way ANOVA followed by Bonferroni's post hoc test. (G) Discrimination index of novel object recognition test performed in *Ptenα*$^{+/+}$ and *Ptenα*$^{mu/mu}$ mice. Data are shown as mean ± SEM, 2-month-old group: $n = 11$ *Ptenα*$^{+/+}$ mice, $n = 12$ *Ptenα*$^{mu/mu}$ mice; 6-month-old group: $n = 8$ *Ptenα*$^{+/+}$ mice, $n = 9$ *Ptenα*$^{mu/mu}$ mice; 12-month-old group: $n = 7$ *Ptenα*$^{+/+}$ mice, $n = 7$ *Ptenα*$^{mu/mu}$ mice. p Values are determined by two-way ANOVA followed by Bonferroni's post hoc test. *$p < .05$, ***$p < .005$, ****$p < .0001$. See also Figure S1

was given 24-h after sample training. The discrimination index declined progressively with increasing age in both *Ptenα*$^{+/+}$ and *Ptenα*$^{mu/mu}$ mice (Figure 2G). However, as compared to age-matched controls, mild cognitive decline was occurred in 2-month-old *Ptenα*$^{mu/mu}$ mice (Figure 2G, 2-month-old). At the age of 6- or 12-month-old, in comparison with age-matched *Ptenα*$^{mu/mu}$ mice, *Ptenα*$^{+/+}$ controls clearly spent more time exploring the novel object as reflected by higher discrimination index (Figure 2G, 6- and 12-month-old), indicating that Ptenα depletion accelerates the rate of cognitive decline with increasing age. Both *Ptenα*$^{+/+}$ and *Ptenα*$^{mu/mu}$ mice showed no evidence of preference for one object over the other (Figure S1C). There was no difference between age matched *Ptenα*$^{+/+}$ and *Ptenα*$^{mu/mu}$ mice in the amount of time on exploring the objects during the sample phase (Figure S1D). In addition, Ptenα deletion has no effects on locomotor activity (Figure S1E).

3.3 | PTENα promotes oxidative metabolism through COX4

In order to determine the cause of increment of oxidative stress in PTENα deficient cells and mice, we re-analyzed the protein profiling data obtained from the brain tissues of *Ptena*$^{+/+}$ and *Ptena*$^{mu/mu}$ mice[32] and mainly focused on the proteins associated with the mitochondrial function. The levels of multiple proteins were decreased in *Ptena*$^{mu/mu}$ mice when compared to those in *Ptena*$^{+/+}$ controls (Table S1). Among them, the subunit of cytochrome c oxidase (COX) COX4 attracted our attention. We first measured the response of endogenous COX4 under stress by immunoblotting with a commercial COX4 antibody. COX4 levels in PTENα$^{+/+}$ cells increased following H_2O_2 treatment, whereas it remained unchanged in PTENα$^{-/-}$ cells (Figure 3A,B), indicating PTENα is required for the upregulation of COX4 upon oxidative stress. Moreover, the evaluation of COX4 levels in cells (Figure 3C, lane 2 vs. lane 1, and Figure 3D) and the midbrain tissues (Figure 3E) showed that PTENα deletion led to a remarkable decrease in COX4 levels. These results infer that PTENα and COX4 participate in the same stress response pathway.

The requirement of COX4 for oxidative metabolism was next determined. We generated COX4 haplo-insufficient (COX4$^{+/-}$) cells by CRISPR/Cas9 (Clustered regularly interspaced short palindromic repeats/caspase-9) technology (Figure S2A). Immunoblotting for COX4 in COX4$^{+/-}$ cells further validated the efficiency of COX4 knockdown (Figure S2B). The ROS levels in COX4$^{+/+}$ and COX4$^{+/-}$ cells were examined by DHE staining, and there was a significant increase in red fluorescence intensity in COX4$^{+/-}$ cells (Figure S2C,D) consistent with the increase caused by PTENα deletion (Figure 1G,H), revealing COX4 knockdown caused abnormal oxidative stress. Re-introduction of exogenous COX4 was sufficient to inhibit ROS enhancement in COX4$^{+/-}$ cells (Figure

FIGURE 3 PTENα regulates oxidative metabolism through COX4. (A) Immunoblot analysis of the indicated proteins in response to H_2O_2 treatment in PTENα$^{+/+}$ and PTENα$^{-/-}$ Hela cells. Blots are representative of 3 independent experiments. (B) Relative protein levels of COX4 in PTENα$^{+/+}$ and PTENα$^{-/-}$ Hela cells treated as indicated normalized to Lamin B. Data in (B) are means ± SEM from 3 independent experiments. *p* Values are determined by two-way ANOVA followed by Bonferroni's post hoc test. (C) Immunoblot analysis of COX4 in PTENα$^{+/+}$ and PTENα$^{-/-}$ Hela cells. Blots are representatives of 3 independent experiments. (D) Quantification of the abundance of COX4 in PTENα$^{+/+}$ and PTENα$^{-/-}$ Hela cells normalized to α-tubulin. Data in (D) are means ± SEM from 3 independent experiments. *p* Values are determined by unpaired *t* test. (E) Representative immunoblots of COX4 and GAPDH in the midbrain of *Ptenα*$^{+/+}$ and *Ptenα*$^{mu/mu}$ mice (left). Quantification of the abundance of COX4 in *Ptenα*$^{+/+}$ and *Ptenα*$^{mu/mu}$ mice normalized to GAPDH (right). Data are means ± SEM, Mice $n = 5$ per genotype. *p* Values are determined by paired *t* test. (F) Representative images of DHE staining to assess ROS levels in PTENα$^{-/-}$ Hela cells containing pSA-N or pSA-COX4. Scale bar, 100 μm. (G) Immunoblot analysis of the indicated proteins in PTENα$^{-/-}$ Hela cells expressing pSA-N or pSA-COX4. Blots are representative of 3 independent experiments. (H) Quantification of ROS levels in PTENα$^{-/-}$ Hela cells containing pSA-N and pSA-COX4 was achieved by measuring mean optical density of DHE signal using image J software. Data in (H) are means ± SEM, $n = 3$ independent experiments with 1.5×10^4 cells in total from PTENα$^{-/-}$ Hela cells containing pSA-N and pSA-COX4 respectively. *p* Values are determined by unpaired *t* tests. (I) COX activity was quantified in mitochondria extracted from PTENα$^{+/+}$, and PTENα$^{-/-}$ cells expressing pSA-N or pSA-COX4. Data are shown as means ± SEM, $n = 3$ independent experiments. *p* Values are determined by one-way ANOVA followed by Turkey's post hoc test. (J) ATP levels reflected by relative luminescence unit (RLU) were quantified in mitochondria extracted from PTENα$^{+/+}$, and PTENα$^{-/-}$ cells expressing pSA-N or pSA-COX4. Data are shown as means ± SEM, $n = 3$ independent experiments. *p* Values are determined by one-way ANOVA followed by Turkey's post hoc test. (K) COX activity was quantified in mitochondria extracted from the midbrain tissues of 1-month-old *Ptenα*$^{+/+}$ and *Ptenα*$^{mu/mu}$ mice. Data are shown as means ± SEM, mice $n = 3$ per genotype. *p* Values are determined by unpaired *t* tests. (L) ATP levels were quantified in mitochondria extracted from the midbrain tissues of 1-month-old *Ptenα*$^{+/+}$ and *Ptenα*$^{mu/mu}$ mice. Data are shown as means ± SEM, mice $n = 5$ per genotype. *p* Values are determined by unpaired *t* tests. (M) ATP levels were quantified with mitochondria extracted from PTENα$^{+/+}$ and PTENα$^{-/-}$ cells treated as indicated. Data are shown as means ± SEM, $n = 3$ independent experiments. *p* Values are determined by two-way ANOVA followed by Tukey's post hoc test. *$p < .05$, **$p < .001$, ***$p < .005$, ****$p < .0001$

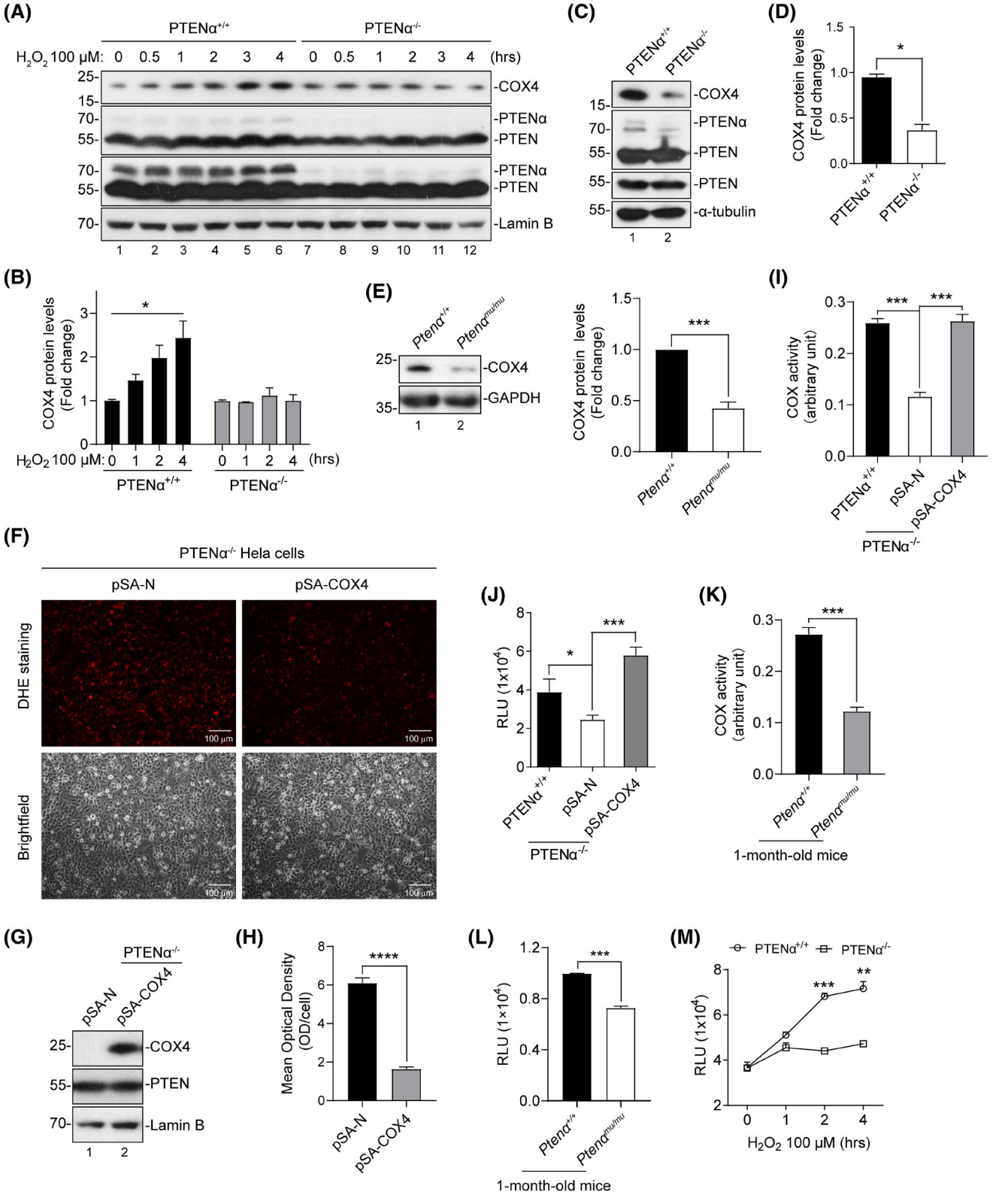

S2E–G), validating the specificity of CRISPR/cas9 targeting. We sought to further elucidate the relationship between PTENα and COX4. Exogenous COX4 was transfected into PTENα$^{-/-}$ Hela cells, and ROS levels reflected by red fluorescence were reduced (Figure 3F–H), suggesting that COX4 is a potential downstream target of PTENα.

As a subunit of COX, COX4 is responsible for COX assembling and its activity is critical for ROS generation and ATP production.[36] As expected, there was an obvious reduction of mitochondrial COX activity and ATP production in PTENα$^{-/-}$ cells (Figure 3I,J, column 2 vs. column 1) and COX4$^{+/-}$ cells (Figure S2H,I), and these defects

in PTENα$^{-/-}$ cells could be sufficiently rescued by introduction of COX4 (Figure 3I,J, column 3 vs. column 2). Consistent results were obtained in mitochondria samples extracted from mouse midbrain tissues. COX activity and ATP levels in *Ptenα*$^{mu/mu}$ mice were significantly less than those in *Ptenα*$^{+/+}$ controls (Figure 3K,L). ATP production upon oxidative stress were assessed in PTENα$^{+/+}$ and PTENα$^{-/-}$ Hela cells. Flowing H_2O_2 treatment, cells tend to produce more ATP to cope with the adverse conditions in PTENα$^{+/+}$ cells, whereas, in the absence of PTENα, ATP levels remained constant (Figure 3M), indicating that PTENα is requisite for the generation of ATP under stress.

Taken together, these results strongly suggest that Ptenα ablation results in the reduction of COX4 levels, which further leads to impairments of COX activity, ATP production, and oxidative metabolism.

3.4 | PTENα protects COX4 from being degraded by NEDD4L

We also attempted to understand the mechanism underlying PTENα regulation of COX4 levels. Reverse transcription-quantitative PCR (qRT-PCR) analysis performed in PTENα$^{+/+}$ and PTENα$^{-/-}$ Hela cells (Figure S3A) and the midbrain tissues of *Ptenα*$^{+/+}$ and *Ptenα*$^{mu/mu}$ mice (Figure S3B) did not produce significant differences in the mRNA levels of COX4, suggesting PTENα regulates COX4 at the post-translational level. We then wondered whether the regulation of COX4 dependents on the phosphatase activity of PTENα. To investigate this, PTENα^{C297S}, a protein and lipid phosphatase dead form of PTENα, together with PTENα and PTEN was separately transfected into PTENα$^{-/-}$ Hela cells, and endogenous COX4 was evaluated. Under the basal condition, none of these proteins affect COX4 levels (Figure 4A, lanes 2–4 vs. lane 1, and Figure 4B). However, PTENα and PTENα^{C297S} but not PTEN increased the expression levels of COX4 upon H_2O_2 stimulation (Figure 4A, lanes 6–8 vs. lane 5, and Figure 4B), indicating that PTENα regulates COX4 in a phosphatase independent manner.

With the application of the proteasome inhibitor MG132, COX4 levels were largely restored in PTENα$^{-/-}$ cells (Figure 4C, lane 4 vs. lane 2, and Figure 4D), which was equivalent to those in PTENα$^{+/+}$ cells (Figure 4C, lane 4 vs. lane 3, and Figure 4D). Furthermore, in the presence of the protein synthesis inhibitor cycloheximide (CHX), COX4 in PTENα$^{-/-}$ cells displayed an obviously shortened

FIGURE 4 PTENα maintains COX4 levels by competitively interacting with NEDD4L under stress. (A) Immunoblot analysis of the indicated proteins in PTENα$^{-/-}$ Hela cells transfected with PTENα, PTENα^{C297S}, or PTEN with or without 100 μM H_2O_2 for 3 h. Blots are representative of 3 independent experiments. (B) Quantification of COX4 levels in PTENα$^{-/-}$ Hela cells transfected with PTENα, PTENα^{C297S}, or PTEN normalized to GAPDH. Cells were treated as indicated. Data are shown as means ± SEM, $n = 3$ independent experiments. p Values are determined by two-way ANOVA followed by Bonferroni's post hoc test. (C) Immunoblot analysis of the indicated proteins in PTENα$^{+/+}$ and PTENα$^{-/-}$ Hela cells incubated with 10 μM proteasome inhibitor MG132 for 0 or 8 h. Blots are representative of 3 independent experiments. (D) Quantification of COX4 levels in PTENα$^{+/+}$ and PTENα$^{-/-}$ Hela cells treated as indicated normalized to GAPDH. Data in (D) are means ± SEM, $n = 3$ independent experiments. p Values are determined by two-way ANOVA followed by Tukey's post hoc test. (E) Immunoblot analysis for COX4, PTENα, PTEN, and GAPDH performed with lysates from PTENα$^{+/+}$ and PTENα$^{-/-}$ Hela cells treated as indicated. Blots are representative of 3 independent experiments. (F) Quantification of COX4 levels in PTENα$^{+/+}$ and PTENα$^{-/-}$ Hela cells treated as indicated normalized to GAPDH. Data in (D) are means ± SEM, $n = 3$ independent experiments. p Values are determined by two-way ANOVA followed by Tukey's post hoc test. (G) Cell lysates from HEK293T cells containing pcs107-HA, NEDD4L-HA, STUB1-HA, NEDD4-HA, GNB2-HA, UBE4B-HA, and UBE4A-HA were immunoblotted for COX4, a-tubulin, and HA. NEDD4L, NEDD4 like E3 ubiquitin protein ligase; STUB1, STIP1 homology and U-Box containing protein 1; NEDD4, NEDD4 E3 ubiquitin protein ligase; GNB2, G protein subunit beta 2; UBE4B, Ubiquitination factor E4B; UBE4A, Ubiquitination factor E4A. Blots are representative of 2 independent experiments. (H) Immunoblot analysis of COX4, NEDD4L, and α-tubulin in PTENα$^{+/+}$ HeLa cells transfected with shRNA oligonucleotide targeting NEDD4L. Blots are representative of 3 independent experiments. (I) Quantification of COX4 levels normalized to α-tubulin in PTENα$^{+/+}$ HeLa cells transfected with shRNA oligonucleotide targeting NEDD4L. Data are shown as means ± SEM, $n = 3$ independent experiments. p Values are determined by unpaired t tests. (J) COX4 ubiquitination levels were evaluated with cell lysates from HEK293T cells co-transfected with HA-His-Ubiquitin (Ub), HA-Stag-COX4, Myc-NEDD4L, and Flag-PTENα as indicated. Cell lysates were prepared under denaturing conditions (Cells lysates were added with SDS to a final concentration 1% and then boiled for 15 min at 95°C) and immunoprecipitated with S-protein beads, and S-protein immunoprecipitants were immunoblotted for HA, Myc, Flag, and a-tubulin. Blots are representative of 3 independent experiments. SDS, sodium dodecyl sulfate. (K) Cell lysates from PTENα$^{+/+}$ Hela cells containing Myc-NEDD4L or Myc-NEDD4L+Flag-PTENα were immunoblotted for COX4, Myc, Flag, and α-tubulin. Blots are representative of 3 independent experiments. (L) Quantification of COX4 levels in PTENα$^{+/+}$ Hela cells containing Myc-NEDD4L or Myc-NEDD4L+Flag-PTENα normalized to α-tubulin. Data in (L) are means ± SEM, $n = 3$ independent experiments. p Values are determined by one-way ANOVA followed by Turkey's post hoc test. (M, N) Reciprocal exogenous binding of PTENα, COX4 and NEDD4L in HEK293T cells. S-tagged-COX4 co-transfected with Myc-mock, Myc-NEDD4L, or Myc-NEDD4L+Flag-PTENα, was pulled-downed with anti-Myc-beads or S-protein beads. Myc or S-protein immunoprecipitants were immunoblotted for Flag, Myc, and HA. Blots are representative of 3 independent experiments. *$p < .05$, **$p < .001$, ***$p < .005$. See also Figure S3

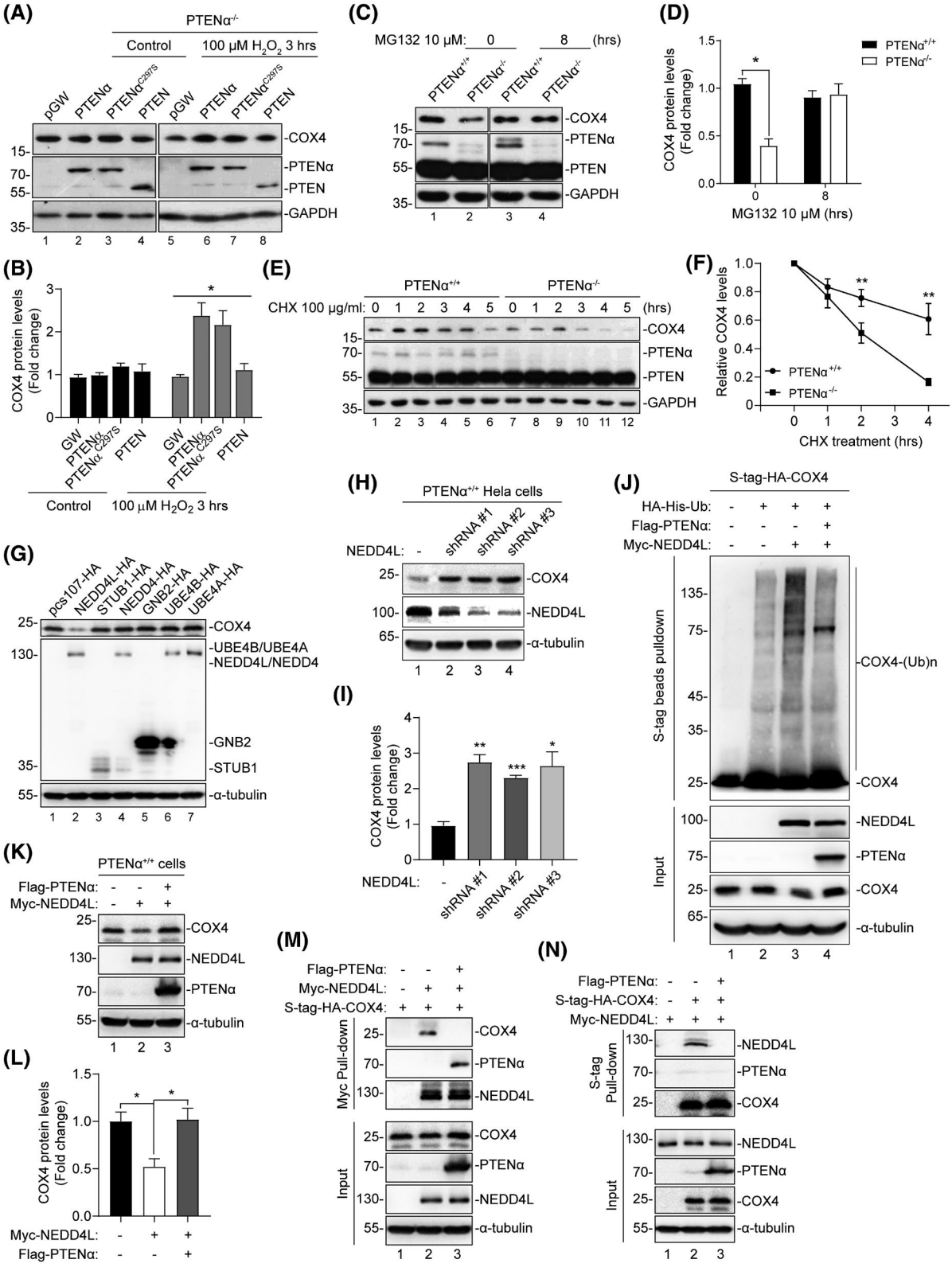

protein half-life as compared to that in PTENα$^{+/+}$ cells (Figure 4E, lanes 1–6 vs. lanes 7–12, Figure 4F, and Figure S3C). These data suggest that PTENα is involved in the maintenance of COX4 protein stability.

These findings raised a question as to whether PTENα and COX4 interact, and this was assessed in HEK293T cells containing Flag-PTENα and HA-S-tag-COX4. PTENα showed no obvious interaction with COX4 either under normal condition or under stress (Figure S3D), indicating PTENα regulates COX4 in an indirect way. To find out the mediator between PTENα and COX4, the prediction of the E3 ligase of COX4 was carried out on the website:

ubibrowser.ncpsb.org. Based on the scores, top 19 of the predicted E3 ligases were listed in Table S2, and displayed as the predicted E3-COX4 network (Figure S3E). To identify the E3 ligase accounting for COX4 degradation, we performed a further screening and top 6 of the predicted E3 ligases were included. Each E3 ligase was separately transfected into HEK293T cells and the endogenous COX4 levels were evaluated. This screening led us to find that NEDD4L remarkably reduced COX4 expression level (Figure 4G, lane 2 vs. lane 1). Other E3 ligases, including STUB1, NEDD4, GNB2, UBE4B, UBE4A, did not affect the expression levels of COX4 (Figure 4G, lanes 3–7 vs. lane 1). Moreover, the depletion of NEDD4L with shRNA markedly increased COX4 levels in PTENα$^{+/+}$ Hela cells (Figure 4H, lanes 2–4 vs. lane 1, and Figure 4I). Subsequently, the possibility that NEDD4L ubiquitylates COX4 was examined. HA-His-tagged Ub was co-transfected with HA-S-tag-COX4, ubiquitylated COX4 was detected by anti-HA immunoblotting of S-tag pull-down under denaturing conditions. NEDD4L increased the ubiquitination levels of COX4 in HEK293T cells (Figure 4J, lane 3 vs. lane 2). In addition, we generated a COX4^{6KR} mutant in which 6 ubiquitinated lysine sites (K) in COX4 identified in previous proteome-screening studies were all replaced by arginine (R), specifically, K29, K53, K135, K149, K159, and K164.[37–39] The ubiquitination assay performed with the COX4^{6KR} mutant showed that NEDD4L cannot affect the ubiquitination levels of COX4^{6KR} (Figure S3F, lane 3 vs. lane 2). These results suggest that NEDD4L is a E3 ubiquitin ligase of COX4 that ubiquitinates and degrades COX4.

We wondered the relationship among COX4, NEDD4L, and PTENα. We found that additional introduction of PTENα remarkably diminished the NEDD4L-mediated COX4 ubiquitination (Figure 4J, lane 4 vs. lane 3), and the ectopic expression of PTENα was sufficient to restore COX4 levels (Figure 4K, lane 3 vs. lane 2, and Figure 4L), demonstrating PTENα counteracts the effect of NEDD4L on COX4. Reciprocal co-immunoprecipitation (co-IP) assays performed in HEK293T expressing HA-S-tag-COX4 and Myc-NEDD4L showed COX4 bound to NEDD4L (Figure 4M, lane 2 vs. lane 1, and Figure 4N, lane 2 vs. lane 1). However, in the presence of PTENα, PTENα competitively interacted with NEDD4L (Figure 4M, lane 3 vs. lane 2, and Figure 4N, lane 3 vs. lane 2), which led to a disruption of COX4-NEDD4L association.

Taken together, these results elucidate that NEDD4L binds to COX4 for further proteasomal degradation, and PTENα protects COX4 from being degraded by NEDD4L through competitively interacting with NEDD4L.

3.5 | PTENα p.H169N is predicted to alter protein function

Point mutation c.C505A, p.H169N, which was identified in PD patients, is a missense mutation that locates in the specific N-terminus of PTENα.[33] We would like to determine whether this mutation altered the capacity of PTENα to regulate COX4. Exogenous PTENα and PTENα^{H169N} mutants were separately transfected into PTENα$^{-/-}$ Hela cells, and the endogenous expression

FIGURE 5 PTENα^{H169N} loses the capability to regulate COX4. (A) Cell lysates from PTENα$^{-/-}$ Hela cells transfected with pGW-control, Flag-PTENα, or Flag-PTENα^{H169N} were immunoblotted for COX4, GAPDH, and Flag. Cells were incubated with 100 μM H_2O_2 for 3 h. Blots are representative of 3 independent experiments. (B) Quantification of the abundance of COX4 in PTENα$^{-/-}$ Hela cells containing pGW-control, Flag-PTENα, or Flag-PTENα^{H169N}, cells were treated with 100 μM H_2O_2 for 3 h. Data are shown as means ± SEM, $n = 3$ independent experiments. p Values are determined by unpaired t tests. (C) Cell lysates from HEK293T cells expressing Myc-NEDD4L, Flag-PTENα, or Flag-PTENα^{H169N} as indicated were immunoprecipitated with Flag-beads, cell lysates and immunoprecipitants were immunoblotted for Myc, Flag, and α-tubulin. Blots are representative of 2 independent experiments. (D) Schematic illustration of AAV expression vectors carrying GFP, PTENα, or PTENα^{H169N}. AAV, adeno-associated virus. (E) Representative green fluorescence images to show the distribution of GFP, GFP-PTENα, or GFP-PTENα^{H169N} in the brain cryosections from *Ptenα*$^{mu/mu}$ mice. (F) Discrimination index (right) and exploration time (left) of novel object recognition (NOR) test in *Ptenα*$^{mu/mu}$ mice expressing GFP (mice $n = 7$), PTENα (mice $n = 6$), and PTENα^{H169N} (mice $n = 7$). Data are shown as means ± SEM. p Values are determined by unpaired t tests. (G) Latency to fall of *Ptenα*$^{mu/mu}$ mice containing GFP (mice $n = 7$), PTENα (mice $n = 6$), or PTENα^{H169N} (mice $n = 7$) in rotarod test. Data in (G) are means ± SEM. p Values are determined by unpaired t tests. (H) Representative images from DHE stained midbrain sections of *Ptenα*$^{mu/mu}$ mice injected with GFP, PTENα, or PTENα^{H169N}. Scale bar, 50 μm. Mice $n = 3$ per group. (I) Schematic indication of mouse midbrain marked with pink. (J) ATP levels were quantified in mitochondria extracted from the midbrain tissues of *Ptenα*$^{mu/mu}$ mice containing GFP, PTENα, or PTENα^{H169N}. Data are shown as means ± SEM, mice $n = 6$ per group. p Values are determined by unpaired t tests. (K) Representative immunoblot analysis of the indicated proteins in the midbrain of *Ptenα*$^{mu/mu}$ mice containing ectopic GFP, PTENα, or PTENα^{H169N}. (L) Quantification of COX4 levels in the midbrain tissues of *Ptenα*$^{mu/mu}$ mice containing ectopic GFP, PTENα, or PTENα^{H169N}. Data are presented as mean ± SEM, mice $n = 3$ per group. p Values are determined by unpaired t tests. (M) Schematic illustration of PTENα in regulation of oxidative metabolism. Under oxidative stress, PTENα competitively interacts with NEDD4L to protect COX4 from being degraded by NEDD4L, then Complex IV activity is enhanced to cope with maladaptive oxidative stress. PTENα loss leads to COX4 reduction and further impaired Complex IV activity, ultimately resulting in cell death and behavioral defects. *$p < .05$, **$p < .001$

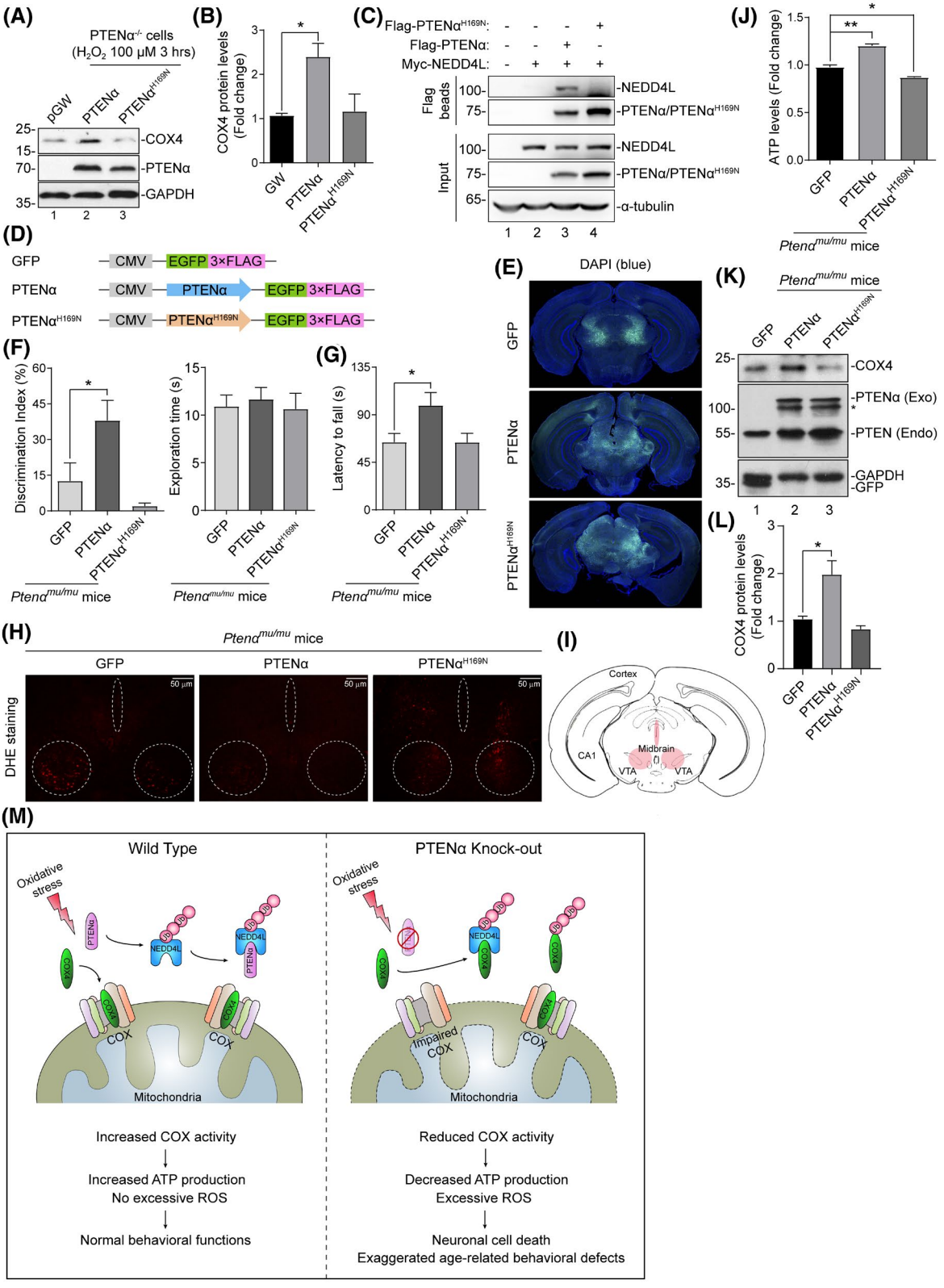

of COX4 was examined under stress. The result showed PTENα increase COX4 levels (Figure 5A, lane 2 vs. lane 1, and Figure 5B), whereas PTENα^{H169N} had no effect (Figure 5A, lane 3 vs. lane 1, and Figure 5B). The underlying mechanism was further explored by co-IP. According to the result, the PTENα^{H169N} mutant failed to bind with NEDD4L (Figure 5C, lane 4 vs. lane 3 vs. lane 2). Our results suggest that the PTENα^{H169N} mutant loses capability to protect COX4.

To explore the impacts of PTENα^{H169N} in vivo, we bilaterally injected AAV containing GFP, human PTENα, or PTENα^{H169N} cDNA into the midbrain of 5-month-old

Ptenα$^{mu/mu}$ mice (Figure 5D). Mice were analyzed 4 weeks after injection, and the fluorescent detection showed exogenous GFP, PTENα, or PTENα^{H169N} mainly distributed in the midbrain (Figure 5E). Behavioral tests were then performed to evaluate the behavioral impacts of GFP, PTENα, and PTENα^{H169N} in *Ptenα*$^{mu/mu}$ mice. In NOR tasks, as compared to mice with GFP or PTENα^{H169N}, mice containing PTENα spent more time on the novel object than the familiar one, as reflected by higher discrimination index (Figure 5F). Consistently, mice carrying GFP or PTENα^{H169N} showed no difference in rotarod tests, whereas mice containing PTENα exhibited an increase in time of latency to fall (Figure 5G). Taken together, these data suggest that the introduction of PTENα but not PTENα^{H169N} in the midbrain alleviates the behavioral deficits in *Ptenα*$^{mu/mu}$ mice.

We further determined whether PTENα or PTENα^{H169N} could ameliorate pathological changes in *Ptenα*$^{mu/mu}$ mice. DHE staining results showed that PTENα re-expression in the midbrain of *Ptenα*$^{mu/mu}$ mice reduced the ROS levels; however, mice containing GFP or PTENα^{H169N} exhibited no difference in ROS levels as reflected by comparable red fluorescence intensity (Figure 5H,I). Moreover, as compared to GFP controls, ATP production was promoted by PTENα, it was noteworthy that ATP production was inhibited by PTENα^{H169N} (Figure 5J). Finally, immunoblotting with midbrain tissues showed that PTENα^{H169N} could not increase the expression level of COX4 (Figure 5K, lane 3 vs. lane 1, and Figure 5L); these results were consistent with that obtained in cells (Figure 5A,B). These data argue that PTENα^{H169N} fails to ameliorate the impairment of ATP production and oxidative metabolism through regulating COX4 in *Ptenα*$^{mu/mu}$ mice.

Taken together, our work demonstrates that, under the normal condition, COX4 is degraded by NEDD4L. However, under oxidative stress, PTENα responsively functions as a protector to protect COX4 through competitively interacting with NEDD4L, further promotes COX activity and ATP production, and maintains the efficient antioxidant process. However, dysregulation of PTENα-mediated signaling results in elevation of oxidative stress, which ultimately leads to cell death and aged-related behavioral defects (Figure 5M).

4 | DISCUSSION

Neurodegenerative disorders are diseases related to multiple factors, patients suffering from which represent a train of behavioral, cognitive, and emotional deterioration.[40] Although it seriously affects people's life quality, the underlying mechanisms remain unclear, and we have not yet found effective therapies. Aging is known to be the greatest risk factor contributing to the neurodegenerative diseases. In this study, we used the Ptenα knockout mouse model to provide a mechanism illustrating the role of PTENα to cope with exaggerated oxidative stress during the aging process. Our data showed that depletion of PTENα resulted in COX activity impairment as well as ROS abnormal accumulation, which led to accelerated defects in age-related behavioral dysfunctions, indicating the cause of oxidative stress during aging is likely due to the impairment of the PTENα-mediated stress response pathway.

A previous study of the impact of PTENα deletion on the mitochondrial respiratory chain showed that the activity of complexes I and III remained unchanged, while the activity of complex IV (COX activity) was impaired in PTENα depleted cells.[31] However, they have failed to interpret the direct mechanism underlying the impairment of COX activity and to consider the physiological/pathological significance of the absence of COX activity in vivo. Our current study aims to provide more data to address these questions. We demonstrate that PTENα maintains COX activity through stabilizing COX4 levels and the impairment of COX activity leads to accelerate brain aging in vivo. The PTENα-mediated stress response pathway is therefore an important mechanism that protects cells from stress-induced damage. Moreover, PTENα^{H169N} failed to rescue phonotypes caused by Ptenα deletion in mice, indicating the loss of function of PTENα^{H169N}. Data also showed that PTENα^{H169N} results in much less ATP levels than those in the GFP group (Figure 5J), suggesting that PTENα^{H169N} might gain some new functions, which are worth being explored in the future.

It is reported that Ptenα ubiquitously distributed in different regions of the brain,[32] whereas we only observed remarkable elevations of ROS levels and cell death in the midbrain of *Ptenα*$^{mu/mu}$ mice. If the PTENα-mediated stress response pathway was the primary pathway for cell death, our findings raised a question as to why other brain regions of *Ptenα*$^{mu/mu}$ mice do not show any abnormal ROS accumulation and cell death as well. This is likely due to the possibility that the pathways that PTENα participates in vary in brain regions. In the hippocampus, PTENα principally modulates CaMKII signaling to regulate learning and memory.[32] In the OB, PTENα mainly modulates the olfactory function by regulating endocytosis.[33] In this study, PTENα is primarily responsible for regulation of the antioxidant pathway in the midbrain. In addition, the specific roles of PTENα in other brain regions need further exploration.

Inhibition of complex IV induces a significant increase in ROS production[19]; we thus propose that the abnormal ROS levels detected in PTENα$^{-/-}$ Hela cells and *Ptenα*$^{mu/mu}$ mice were attributed to the dysfunction of complex IV. However, Complex IV could not generate ROS directly[41]; therefore, how impaired Complex IV impacts

ROS levels is still undetermined. Complex III is proved to be the major source of mitochondrial ROS production under normal metabolic conditions,[41,42] raising the possibility that Complex IV defects might cause a negative feedback to impact Complex III. On the other hand, with the stimulation of hydrogen peroxide, ATP production was increased to cope with the stress situation, suggesting a greater demand of ATP to defense oxidative stress. Taken together, we hypothesize that the impairment of Complex IV causes abnormalities in two ways: promoting ROS generation in Complex III and reducing the energy supply for ROS clearance, both result in ROS accumulation. This hypothesis needs to be addressed in our future work.

In summary, we have identified that the *PTENα* gene is linked to aging. Our findings reveal the importance of PTENα signaling in protection of neural cells against oxidative stress. Through evaluating effects of *PTENα* depletion and mutation, we characterized a stress-dependent mechanism involving aging. This study may help us to understand the complexity of PTEN family and pave the way for diagnosis and treatment of patients with age-related neurodegenerative diseases.

ACKNOWLEDGEMENTS

We thank Drs. X. Zhao, L. Liang, Z. Hou, Y. Li, J. Gong and J. Yang for technical assistance and Peking-Tsinghua Center for Life Science for postdoctoral funding. This study was supported by the National Natural Science Foundation of China (81430056, 31420103905, 81621063 and 31800849), National Key Research and Development Program of China (2016YFA0500302), Beijing Natural Science Foundation Key Grant (7161007) and the China Postdoctoral Science Foundation (2017M620006).

DISCLOSURES

The authors declare that they have no conflicts of interest with the contents of this article.

AUTHOR CONTRIBUTIONS

Yang Liu and Pan Wang conceived the study and designed the major experiments. Pan Wang performed experiments in behavioral and biological examinations, analyzed the data. Ruiqi Li performed experiments in behavioral examination, plasmid construction, protein interaction related experiments. Yuyao Yuan and Yang Liu sequenced the PD samples and identified the point mutant of PTENα. Minglu Zhu and Yang Liu generated the *Ptena* mutant mice. The manuscript was written by Pan Wang and Yuxin Yin.

REFERENCES

1. Burte F, Carelli V, Chinnery PF, Yu-Wai-Man P. Disturbed mitochondrial dynamics and neurodegenerative disorders. *Nat Rev Neurol*. 2015;11:11-24.
2. Shefa U, Jeong NY, Song IO, et al. Mitophagy links oxidative stress conditions and neurodegenerative diseases. *Neural Regen Res*. 2019;14:749-756.
3. Alexander GE, Ryan L, Bowers D, et al. Characterizing cognitive aging in humans with links to animal models. *Front Aging Neurosci*. 2012;4:21.
4. Dykiert D, Der G, Starr JM, Deary IJ. Age differences in intra-individual variability in simple and choice reaction time: systematic review and meta-analysis. *PLoS ONE*. 2012;7:e45759.
5. Mattson MP, Arumugam TV. Hallmarks of brain aging: adaptive and pathological modification by metabolic states. *Cell Metab*. 2018;27:1176-1199.
6. Papagno C, Trojano L. Cognitive and behavioral disorders in Parkinson's disease: an update. I: cognitive impairments. *Neurol Sci*. 2018;39:215-223.
7. Scheltens P, Blennow K, Breteler MM, et al. Alzheimer's disease. *Lancet*. 2016;388:505-517.
8. Lopez-Otin C, Blasco MA, Partridge L, Serrano M, Kroemer G. The hallmarks of aging. *Cell*. 2013;153:1194-1217.
9. Kujoth GC, Hiona A, Pugh TD, et al. Mitochondrial DNA mutations, oxidative stress, and apoptosis in mammalian aging. *Science*. 2005;309:481-484.
10. Trifunovic A, Wredenberg A, Falkenberg M, et al. Premature ageing in mice expressing defective mitochondrial DNA polymerase. *Nature*. 2004;429:417-423.
11. Vermulst M, Wanagat J, Kujoth GC, et al. DNA deletions and clonal mutations drive premature aging in mitochondrial mutator mice. *Nat Genet*. 2008;40:392-394.
12. Shih AY, Imbeault S, Barakauskas V, et al. Induction of the Nrf2-driven antioxidant response confers neuroprotection during mitochondrial stress in vivo. *J Biol Chem*. 2005;280:22925-22936.
13. Suzuki T, Yamamoto M. Stress-sensing mechanisms and the physiological roles of the Keap1-Nrf2 system during cellular stress. *J Biol Chem*. 2017;292:16817-16824.
14. Stranahan AM, Mattson MP. Recruiting adaptive cellular stress responses for successful brain ageing. *Nat Rev Neurosci*. 2012;13:209-216.
15. Harman D. Free radical theory of aging: an update: increasing the functional life span. *Ann N Y Acad Sci*. 2006;1067:10-21.
16. Renaud J, Simola N, Martinoli MG. The sweet road to Parkinson's disease. *Aging*. 2019;11:853-854.
17. Dai DF, Chiao YA, Marcinek DJ, Szeto HH, Rabinovitch PS. Mitochondrial oxidative stress in aging and healthspan. *Longev Healthspan*. 2014;3:6.
18. Shadel GS, Horvath TL. Mitochondrial ROS signaling in organismal homeostasis. *Cell*. 2015;163:560-569.
19. Sipos I, Tretter L, Adam-Vizi V. Quantitative relationship between inhibition of respiratory complexes and formation of reactive oxygen species in isolated nerve terminals. *J Neurochem*. 2003;84:112-118.
20. Acin-Perez R, Gatti DL, Bai Y, Manfredi G. Protein phosphorylation and prevention of cytochrome oxidase inhibition by ATP: coupled mechanisms of energy metabolism regulation. *Cell Metab*. 2011;13:712-719.
21. Abu-Libdeh B, Douiev L, Amro S, et al. Mutation in the COX4I1 gene is associated with short stature, poor weight gain and increased chromosomal breaks, simulating Fanconi anemia. *Eur J Hum Genet*. 2017;25:1142-1146.
22. Barrientos A, Gouget K, Horn D, Soto IC, Fontanesi F. Suppression mechanisms of COX assembly defects in yeast

and human: insights into the COX assembly process. *Biochim Biophys Acta*. 2009;1793:97-107.
23. Kadenbach B, Ramzan R, Vogt S. Degenerative diseases, oxidative stress and cytochrome c oxidase function. *Trends Mol Med*. 2009;15:139-147.
24. Larsson NG. Somatic mitochondrial DNA mutations in mammalian aging. *Annu Rev Biochem*. 2010;79:683-706.
25. Foti SC, Hargreaves I, Carrington S, Kiely AP, Houlden H, Holton JL. Cerebral mitochondrial electron transport chain dysfunction in multiple system atrophy and Parkinson's disease. *Sci Rep*. 2019;9:6559.
26. Gu M, Cooper JM, Taanman JW, Schapira AH. Mitochondrial DNA transmission of the mitochondrial defect in Parkinson's disease. *Ann Neurol*. 1998;44:177-186.
27. Swerdlow RH, Parks JK, Miller SW, et al. Origin and functional consequences of the complex I defect in Parkinson's disease. *Ann Neurol*. 1996;40:663-671.
28. Huttemann M, Kadenbach B, Grossman LI. Mammalian subunit IV isoforms of cytochrome c oxidase. *Gene*. 2001;267:111-123.
29. Kadenbach B, Huttemann M. The subunit composition and function of mammalian cytochrome c oxidase. *Mitochondrion*. 2015;24:64-76.
30. Hopkins BD, Fine B, Steinbach N, et al. A secreted PTEN phosphatase that enters cells to alter signaling and survival. *Science*. 2013;341:399-402.
31. Liang H, He S, Yang J, et al. PTENalpha, a PTEN isoform translated through alternative initiation, regulates mitochondrial function and energy metabolism. *Cell Metab*. 2014;19:836-848.
32. Wang P, Mei F, Hu J, et al. PTENalpha modulates CaMKII signaling and controls contextual fear memory and spatial learning. *Cell Rep*. 2017;19:2627-2641.
33. Yuan Y, Zhao X, Wang P, et al. PTENalpha regulates endocytosis and modulates olfactory function. *FASEB J*. 2019;33:11148-11162.
34. Clipperton-Allen AE, Page DT. Pten haploinsufficient mice show broad brain overgrowth but selective impairments in autism-relevant behavioral tests. *Hum Mol Genet*. 2014;23:3490-3505.
35. Bredesen DE, Rao RV, Mehlen P. Cell death in the nervous system. *Nature*. 2006;443:796-802.
36. Coenen MJ, van den Heuvel LP, Smeitink JA. Mitochondrial oxidative phosphorylation system assembly in man: recent achievements. *Curr Opin Neurol*. 2001;14:777-781.
37. Kim W, Bennett EJ, Huttlin EL, et al. Systematic and quantitative assessment of the ubiquitin-modified proteome. *Mol Cell*. 2011;44:325-340.
38. Shi Y, Chan DW, Jung SY, Malovannaya A, Wang Y, Qin J. A data set of human endogenous protein ubiquitination sites. *Mol Cell Proteomics*. 2011;10:M110.002089.
39. Wagner SA, Beli P, Weinert BT, et al. A proteome-wide, quantitative survey of in vivo ubiquitylation sites reveals widespread regulatory roles. *Mol Cell Proteomics*. 2011;10:M111.013284.
40. Liu Z, Zhou T, Ziegler AC, Dimitrion P, Zuo L. Oxidative stress in neurodegenerative diseases: from molecular mechanisms to clinical applications. *Oxid Med Cell Longev*. 2017;2017:2525967.
41. Turrens JF. Superoxide production by the mitochondrial respiratory chain. *Biosci Rep*. 1997;17:3-8.
42. Finkel T, Holbrook NJ. Oxidants, oxidative stress and the biology of ageing. *Nature*. 2000;408:239-247.

SUPPORTING INFORMATION

Additional Supporting Information may be found in the online version of the article at the publisher's website.

How to cite this article: Wang P, Li R, Yuan Y, et al. PTENα is responsible for protection of brain against oxidative stress during aging. *FASEB J*. 2021;35:e21943. doi:10.1096/fj.202100753R